




A gray level indicator-based nonlinear diffusion equation for the removal of random-valued impulse noise

Kehan Shi¹ 

Received: 4 March 2021 / Revised: 20 July 2021 / Accepted: 14 January 2022 /
Published online: 16 February 2022

© The Author(s), under exclusive licence to Springer Science+Business Media, LLC, part of Springer Nature 2022

Abstract

This paper proposes a nonlinear diffusion equation with two diffusivities to restore images corrupted by random-valued impulse noise. A Perona–Malik type diffusivity is utilized for anisotropic diffusion and a gray level based diffusivity called gray level indicator is proposed to estimate the amplitude of the noise. Then the proposed equation has a large diffusion coefficient for homogeneous regions and regions corrupted by large impulse noise. Conversely, it has a small diffusion coefficient for regions with edges, fine details, as well as regions corrupted by small impulse noise. The gray level indicator is constructed as the square of the difference between the noisy image and a reference image deduced from median-type filters. The new equation is able to remove small random-valued impulse noise that is difficult to be detected. A robust stopping criteria based on the complexity of the restored image and the noise level is proposed. Numerical experiments show that it outperforms PDE-based methods and nonlocal methods.

Keywords Image denoising · Random-valued noise · Diffusion equation · Gray level indicator

1 Introduction

Due to defected equipment, electromagnetic interference, and interfered channels in acquisition and transmission, digital images are often corrupted by impulse noise [15]. Let u_0 be an original image, where $(u_0)_{i,j}$ is the gray level of u_0 at location (i, j) . The noisy image contaminated by impulse noise is defined by

$$f_{i,j} = \begin{cases} n_{i,j}, & \text{with probability } s, \\ (u_0)_{i,j}, & \text{with probability } 1 - s, \end{cases}$$

where $n_{i,j}$ is the impulse noise and s is the noise level [12]. The problem of image denoising under impulse noise is to find an approximation u of the true image u_0 from the observed

✉ Kehan Shi
kshi@cjlu.edu.cn

¹ Department of Mathematics, China Jiliang University, Hangzhou, 310018 China

noisy image f such that important structures like edges and details are preserved but impulse noise is removed. Two common types of impulse noise are salt-and-pepper noise and the random-valued noise. Assume that the dynamic range of u_0 is $[d_{min}, d_{max}]$. For images corrupted by salt-and-pepper noise, $n_{i,j}$ can take only two values d_{min} and d_{max} , while for images corrupted by random-valued noise, $n_{i,j}$ can take any random value between d_{min} and d_{max} . Generally, random-valued noise is harder to deal with than salt-and-pepper noise. In this paper, we focus on the problem of removing random-valued impulse noise from images.

According to the definition of impulse noise, only a portion of pixels in images are corrupted. Commonly used algorithms for removing impulse noise are the two-stage method, i.e., detection followed by filtering. More precisely, an impulse noise detector is applied to identify corrupted pixels, then different types of filters are employed to restore the corrupted pixels and leave the noise-free pixels unchanged.

Median filter and its variations [10, 11, 19–21, 27] have been widely used in the literature for restoring corrupted pixels. These filters are nonlinear and preserve edges well for low density impulse noise suppression. With the increase of the noise level, the filtering window is getting larger. As a result, edges and some details in images are smeared. The main advantage of the median filter and its variations is the very fast execution speed [2, 19]. Another well-known method for restoring corrupted pixels is the weighted mean filter [14, 17, 18, 23, 30, 45, 47], which exploits the correlation among neighboring pixels to restore the corrupted pixels. Also, it adaptively determines the filtering window and utilizes only uncorrupted pixels for the restoration. Recently, the fuzzy technique was considered to improve the denoising results [3, 9, 12, 22, 26, 32, 39]. In this method, the authors determined how impulse-like a pixel is rather than determining whether it is corrupted. It is well suited for removing random-valued noise since random-valued noise is difficult to detect [13, 25, 40].

It is worth mentioning that many outstanding methods for removing impulse noise are inspired by ideas for removing Gaussian noise. The functional with the total variation (TV) regularization and the L^2 data fitting term is efficient for many image processing problems [5, 31, 33]. By observing that the L^1 norm is more robust in the presence of outliers, TV- L^1 functionals were proposed for removing impulse noise [28, 42]. Recently, TV-nonconvex models were proposed [1, 24, 41, 43, 44, 46] since TV- L^1 model will only lead to a sub-optimal solution. Nonlocal means filter [6] was first introduced to preserve textural information in images. It was also extended for removing impulse noise [12, 35, 39, 40]. The main challenge of applying the nonlocal mean filter to the case of impulse noise is the calculation of the nonlocal weights. In [40], the authors proposed to calculate the nonlocal weights based on a reference image that is obtained by the median filter. The more common approach of calculating the weights is to utilize only the noise-free pixels [12, 35, 39].

Diffusion equations have become a powerful tool for image denoising since the introduction of the Perona-Malik equation [29]. In [38], the authors proposed a PDE (Partial Differential Equation) model based on diffusion coefficients that take different values for interior pixels, edges, and noise pixels. However, the denoising results generally have low quantitative evaluation values and poor visual quality, especially when the noise level is high. In [36], a non-divergence equation was proposed for removing impulse noise, which first detects the noise pixels and then removes these noise by a diffusion equation. The equation, as well as the aforementioned nonlocal methods, are the two-stage method. Consequently, the results depend heavily on the accuracy of the noise detection.

Recently, we proposed a gray level indicator to estimate the amplitude of Cauchy noise in images [34]. Note that both Cauchy noise and random-valued noise have a very impulsive character. In this paper, we modify the gray level indicator to estimate the amplitude of

random-valued noise. A nonlinear diffusion equation is proposed based on the gray level indicator under the framework of diffusion equations in the non-divergence form [34, 36]. By introducing the gray level indicator, we estimate how impulse-like pixels in images are and avoid the step of noise detection. It achieves the goal of fuzzy estimation for random-valued noise [12]. A pixel with a large gray level indicator has a larger diffusion coefficient than a pixel with a small gray level indicator. Consequently, small random-valued impulse noise that is difficult to be detected by two-stage methods can be removed efficiently by the new equation. Finding an appropriate stopping time for diffusion equations is a crucial problem in image processing. We propose a robust stopping criteria based on the complexity of the restored image and the noise level.

The rest of this paper is organized as follows. In Section 2, we discuss details of the proposed equation and the implementation of it for removing random-valued impulse noise. Numerical experiments are provided in Section 3 to demonstrate the efficiency of the equation. We conclude the paper in Section 4.

2 The proposed equation

2.1 Related works and the proposed diffusion equation

Nonlinear diffusion equation

$$\frac{\partial u}{\partial t} = \operatorname{div}(c(|\nabla u|)\nabla u) \quad (1)$$

has attracted a lot of attention in image restoration under Gaussian noise [4]. In many real-world applications, images are often corrupted by non-Gaussian noise that has a very impulsive character. Typical examples include impulse noise and Cauchy noise. In both problems, the gradient-based adaptive edge detector $c(|\nabla u|)$ can not distinguish pixels corrupt by large noise from isolated edges. As a result, (1) fails to remove noise without smearing details of images.

In [36], we proposed to handle impulsive pixels and non-impulse pixels in different ways. To this end, an impulse noise indicator $\lambda(x)$ was introduced for (1), and the equation for removing impulse noise has the following non-divergence form

$$\frac{\partial u}{\partial t} = \lambda(x)\operatorname{div}(c(|\nabla u|)\nabla u). \quad (2)$$

Here $\lambda(x)$ is a characteristic function that equals 1 for noisy pixels and 0 for noise-free pixels. Consequently, only noisy pixels are processed by the equation. As we have mentioned in the introduction, this is a two-stage method, and the results depend heavily on the accuracy of noise detection.

Recently, we proposed a new gray level based diffusivity for the removal of Cauchy noise [34]. The proposed equation has the following form

$$\frac{\partial u}{\partial t} = \left(\frac{|u_0(x) - f(x)|}{\max_{x \in \Omega} \{|u_0(x) - f(x)|\}} \right)^\alpha \operatorname{div}(c(|\nabla u|)\nabla u), \quad (3)$$

where α is a positive parameter. Here the gray level based diffusivity $|u_0 - f|$ estimates the amplitude of the noise. Consequently, the larger the noise, the larger the diffusion coefficient is used in (3). It was verified in [34] that (3) restores the impulsive part of the noisy image efficiently.

We call both $\lambda(x)$ in (2) and $|u_0 - f|$ in (3) the gray level indicator. The difference is that $\lambda(x)$ indicates whether a pixel is corrupted while $|u_0 - f|$ indicates how impulse-like a pixel is. $|u_0 - f|$ can be viewed as the continuous generalization of $\lambda(x)$. They have the same effect for noise-free pixels but a slightly different effect for noisy pixels.

Notice that both Cauchy noise and impulse noise are impulsive. It is straightforward to consider the removal of impulse noise under the framework of (3). Equation (3) has two advantages over (2) for the removal of random-valued noise. First, although both equations have the same effect for noise-free pixels, (3) is able to avoid over smoothness for noisy pixels that have small value $|u_0 - f|$ (see Fig. 1). Second, as we shall see in the next section, (3) is no longer a two-stage method. Consequently, it is able to remove small random-valued noise that is difficult to be detected (see Fig. 6).

The function $c(\cdot)$ needs to be determined in advance. In this paper, we utilize the widely used Perona-Malik type diffusivity [7]

$$c(|\nabla u|) = \frac{1}{1 + (|\nabla u_\sigma|/K)^2}, \quad (4)$$

for (3). Here u_σ is the convolution of u with a Gaussian of standard deviation σ , K is a positive constant. The utilization of convolution for (3) is based on the fact that images corrupted by impulse noise are highly oscillating. The convolution operator smoothes noisy images and reduces the effects of noise on the coefficient [36].

Before proceeding, we compare (3) with (2) through an experiment. Let us assume for a moment that the original image u_0 is given. Then both $\lambda(x)$ and $|u_0 - f|$ are known. We let the noisy image f be the initial condition for (2) and (3), respectively. By evolving these two equations with the homogeneous Neumann boundary condition, the solutions are the denoised images. All the parameters except the iteration numbers in both equations are set as suggested in Section 3.1. Since the original image is given, we manually select the iteration numbers for them such that the PSNR values of the denoised images achieve the highest.

Table 1 lists the PSNR results of (2) and (3) for restoring Boat image corrupted by 10%–90% random-valued noise. We observe that (3) performs better than (2) for all noise levels. The advantage of (3) is becoming more apparent with the increase of the noise

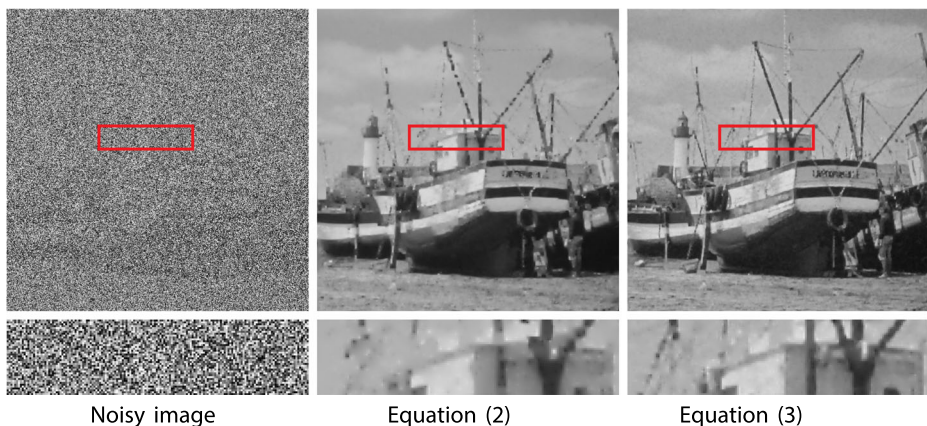


Fig. 1 Denoising results of (2) and (3) for restoring Boat image corrupted by 90% random-valued noise. The second row shows the enlarged subimages

Table 1 PSNR results of (2) and (3) for restoring Boat image corrupted by random-valued noise

	10%	20%	30%	40%	50%	60%	70%	80%	90%
(2)	43.24	39.80	37.24	35.52	33.67	32.06	30.21	28.34	25.57
(3)	43.55	40.20	37.76	36.24	34.64	33.30	31.91	30.56	29.04

level. In Fig. 1, we show the denoising results for Boat image corrupted by 90% random-valued noise. Both equations restore homogeneous regions perfectly. It is observed that (3) outperforms (2) in restoring edges and small details in images.

2.2 Implementation

In the image denoising problem, the original image u_0 is always unknown. Consequently, we need to substitute u_0 in (3) by a reference image v . The final diffusion equation for removing random-valued impulse noise is given by

$$\frac{\partial u}{\partial t} = g(x)\text{div}\left(\frac{1}{1 + (|\nabla u_\sigma|/K)^2} \nabla u\right), \tag{5}$$

where $g(x) = \left(\frac{|v(x)-f(x)|}{\max_{x \in \Omega}\{|v(x)-f(x)|\}}\right)^\alpha$ is the gray level indicator.

By using the half-point scheme [8], (5) can be discretized as

$$u_{i,j}^{(n+1)} = u_{i,j}^{(n)} + \tau g_{i,j} \cdot \left[c_{i+\frac{1}{2},j}^{(n)} \left(u_{i+1,j}^{(n)} - u_{i,j}^{(n)} \right) + c_{i-\frac{1}{2},j}^{(n)} \left(u_{i-1,j}^{(n)} - u_{i,j}^{(n)} \right) + c_{i,j+\frac{1}{2}}^{(n)} \left(u_{i,j+1}^{(n)} - u_{i,j}^{(n)} \right) + c_{i,j-\frac{1}{2}}^{(n)} \left(u_{i,j-1}^{(n)} - u_{i,j}^{(n)} \right) \right], \tag{6}$$

where τ is the time step, $n \geq 0$, $u^{(n)}$ is the denoised image at the n th iteration, $u_{i,j}^{(n)}$ denotes the gray value of $u^{(n)}$ at pixel (i, j) , $u^{(0)} = f$ is the observed noisy image, and

$$g_{i,j} = \left(\frac{|v_{i,j} - f_{i,j}|}{\max\{|v_{i,j} - f_{i,j}|\}}\right)^\alpha,$$

$$c_{i+\frac{1}{2},j}^{(n)} = \frac{1}{1 + \left(|(u_\sigma)_{i+1,j}^{(n)} - (u_\sigma)_{i,j}^{(n)}|/K\right)^2}.$$

$c_{i-\frac{1}{2},j}^{(n)}$, $c_{i,j+\frac{1}{2}}^{(n)}$, and $c_{i,j-\frac{1}{2}}^{(n)}$ are defined in a similar way. Notice that an anisotropic scheme [16, 29] is used for the calculation of the Perona–Malik type diffusivity.

In the rest of this section, we discuss the construction of the reference image v . In the case of Cauchy noise, we can simply use the Gaussian filter and let $v = u_\sigma$. However, it cannot give satisfied results for random-valued noise. A straightforward approach is to restore noisy image f by median type filters. In fact, we are able to use the classical adaptive center-weighted median filter (ACWMF) [10] and the median filter to create v and update v by (5) automatically. The proposed model for removing random-valued noise is summarized in Algorithm 1. The selection of parameters that arose in the algorithm will be discussed in Section 3.1.

Algorithm 1 Remove random-valued noise from images

```

1: Input: Noisy image  $f$ , noise level  $s$ , iteration number  $N$ .
2: Initialization:  $m = 0, v = f$ .
3: while  $m < N$  do
4:   Update  $v$  by applying ACWMF to  $v$ .
5:   Update  $v$  by applying the median filter to  $v$ .
6:   Initialize  $u^{(0)} = f, n = 0$ .
7:   while  $r \leq s$  do
8:     Update  $u^{(n+1)}$  by solving equation (6).
9:     Calculate  $T = \text{Mean}(|u^{(n+1)} - u_{\sigma}^{(n)}|) + \frac{1}{10s}$ .
10:    Count the number  $N_c$  of elements of
         $\{(i, j) \mid |u_{i,j}^{(n+1)} - f_{i,j}| \geq T\}$ .
11:    Calculate  $r = \frac{N_c}{\text{size of } f}$ .
12:     $n = n + 1$ .
13:   end while
14:    $v = u^{(n)}$ .
15:    $m = m + 1$ .
16: end while
17: Output: denoised image  $u^{(n)}$ .

```

In the following, we give some remarks on the details of Algorithm 1. A two-level iterative method is used in Algorithm 1. The reason for updating v in the external iteration is based on the fact that the performance of median type filters drops rapidly with the increase of noise level. Consequently, the updating strategy can improve the denoising results remarkably. In Fig. 2, we illustrate the role of the external iteration. All parameters except N are selected according to the discussion in Section 3.1. When $N = 1$, median type filters can not give a satisfied approximation of the original image. Consequently, the gray level indicator g is not accurate. With the increase of the iteration number N , it can be observed from the figure that both the PSNR value and the visual quality improve by a large margin.

In step 4, we use ACWMF to remove impulse noise in images and obtain the reference image v . The utilization of the median filter in step 5 is based on the observation that ACWMF cannot identify some obvious noisy pixels and pixels with small $|u_0 - f|$, especially when the noise level is high. Another possible approach is to construct v by a state-of-the-art method. But there exists a problem with this approach: If the state-of-the-art

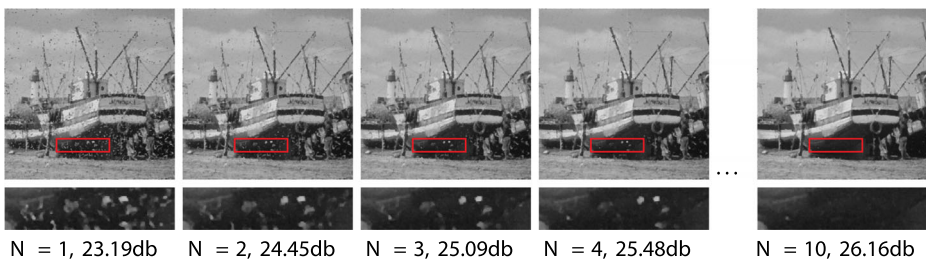


Fig. 2 Denoising results of Algorithm 1 with different N for Boat image corrupted by 60% random-valued noise. The second row are enlarged subimages

method cannot restore pixels with small details and small $|u_0 - f|$, then our algorithm can also not restore these pixels by the given v .

A stopping criteria (step 9-11) is proposed in the internal iteration. The threshold T in step 9 depends on the complexity of the restored image (estimated by the mean value of $|u^{(n+1)} - u_\sigma^{(n)}|$) and the noise level s . We estimate the noise level r according to the given $u^{(n+1)}$ and stop the iteration when $r > s$.

In Fig. 3 we compare the denoising performance of ‘NLM’, ‘Optimal’, and Algorithm 1. Here ‘NLM’ denotes the algorithm that replace the median type filters in step 4-5 of Algorithm 1 by the nonlocal means filter [12]. ‘Optimal’ denotes the algorithm that finds the optimal iteration numbers according to the PSNR value. We observe that NLM performs better than Algorithm 1 in individual cases. Generally, using a state-of-the-art method instead of median-filters to obtain v does not improve the results for our method. It is verified from the results of ‘Optimal’ and our algorithm that the proposed stopping criteria is robust and efficient.

Algorithm 1 contains two parts: calculating the reference image by median-type filters and removing noise by (5). From this point of view, Algorithm 1 is a two-stage method. However, we prefer not to regard our method as a two-stage method, since there exist essential differences between Algorithm 1 and the existing two-stage method, which utilizes the approach of detection followed by filtering.

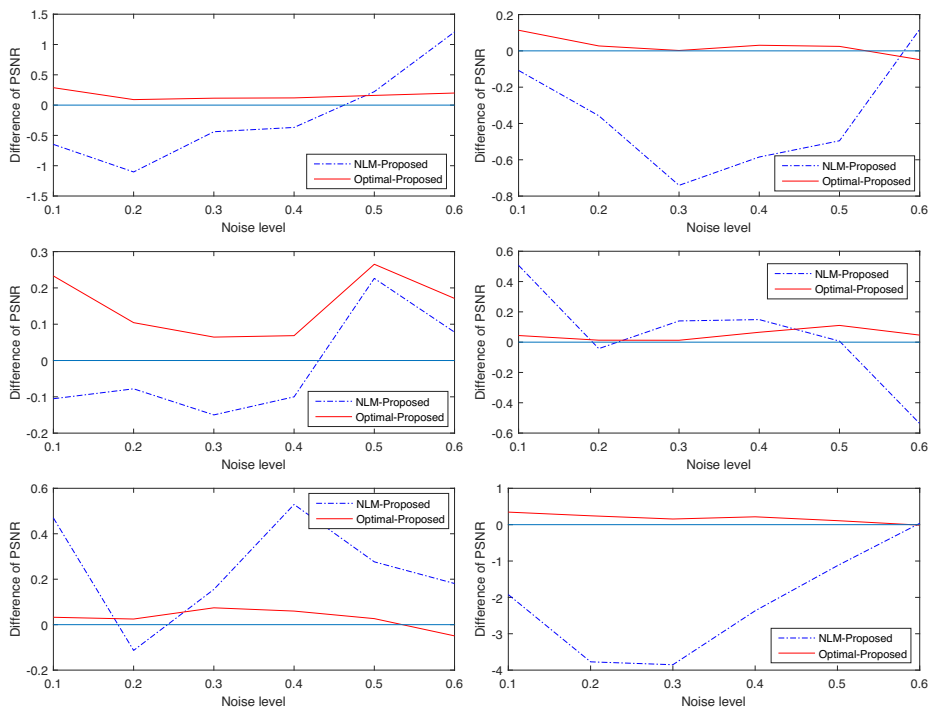


Fig. 3 Denoising results of NLM and the proposed equation for six test images (see Fig. 4). From left to right, from top to bottom: Pepper, Boat, Bridge, Mandrill, Couple and Plane. Legend ‘NLM-Proposed’ (‘Optimal-Proposed’, respectively) denotes the difference of PSNR between NLM and the proposed equation (Optimal and the proposed equation, respectively)

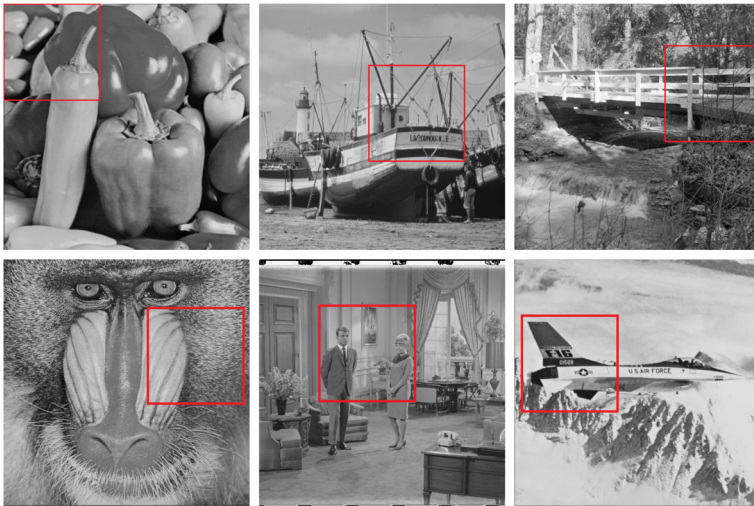


Fig. 4 Test images Pepper, Boat, Bridge, Mandrill, Couple and Plane. The regions in red squares will be displayed in Fig. 5 and Fig. 6 for better visual comparison

3 Numerical experiments

In this section, numerical results are presented to demonstrate the performance of the proposed equation for removing random-valued noise in images. Six commonly used 512×512 8-bit depth test images from the USC-SIPI Image Database¹, which are shown in Fig. 4, are selected for simulations. Peak Signal-to-Noise Ratio (PSNR) and Structural-SIMilarity (SSIM) index [37] are employed for the quantitative evaluation of the denoised images. The following algorithms are considered for the comparison.

- NSDD, a PDE-based method that takes different values of diffusion coefficients for interior pixels, edges, and noise pixels [38].
- AOP, the TV blind inpainting using adaptive outlier pursuit [41]. For the regularization parameter λ , we swept over

$$\{10, 50, 100, 500, 1000, 5000, 10000, 50000\}$$

and choose the best one for each test image and each noise level.

- LOTV, a sparse optimization method based on the l_0 -norm and the TV regularization [43]. For the regularization parameter λ , we swept over $\{0.1, 0.6, 0.11, \dots, 9.6\}$ and choose the best one for each test image and each noise level.
- ROR-NLM, A two-stage method based on the nonlocal means filter [40]. The nonlocal weights are calculated by reference images.
- SAFE, a two-stage method. It detects random-valued noise by the iterative structure-adaptive fuzzy estimation and restores corrupted pixels by the nonlocal means filter [12].

The codes of NSDD and LOTV are available on the original authors' webpages. The code of AOP and SAFE are provided by the original authors. All parameters of the five methods

¹<http://sipi.usc.edu/database/database.php>

Table 2 PSNR and SSIM values of restoration results for images corrupted by random-valued noise

Image	Method	PSNR					SSIM						
		10%	20%	30%	40%	50%	60%	10%	20%	30%	40%	50%	60%
Pepper	NSDD	35.54	33.44	31.82	30.41	28.43	25.53	0.9834	0.9752	0.9615	0.9455	0.9116	0.8218
	AOP	38.83	36.10	33.61	30.79	28.53	26.09	0.9973	0.9922	0.9804	0.9519	0.9203	0.8756
	LOTV	35.99	34.01	32.50	30.93	29.25	26.40	0.9924	0.9870	0.9804	0.9688	0.9507	0.8994
	ROR-NLM	34.51	33.54	32.71	31.71	30.42	28.40	0.9905	0.9869	0.9827	0.9761	0.9660	0.9438
	SAFE	35.31	34.59	33.81	32.35	30.85	28.55	0.9910	0.9895	0.9862	0.9773	0.9669	0.9370
	Algorithm 1	39.37	36.77	34.82	33.11	31.06	28.17	0.9958	0.9928	0.9880	0.9806	0.9669	0.9378
Boat	NSDD	32.57	30.78	29.12	27.74	26.03	24.21	0.9766	0.9592	0.9387	0.9104	0.8592	0.7676
	AOP	34.95	32.27	29.85	27.98	26.30	24.47	0.9908	0.9798	0.9525	0.9106	0.8590	0.7883
	LOTV	29.40	28.41	27.55	26.75	25.72	24.59	0.9541	0.9396	0.9231	0.9024	0.8713	0.8206
	ROR-NLM	32.37	30.15	28.63	28.03	26.97	25.78	0.9759	0.9565	0.9399	0.9300	0.9109	0.8810
	SAFE	32.52	31.52	30.08	28.98	27.14	25.93	0.9787	0.9726	0.9605	0.9457	0.9051	0.8700
	Algorithm 1	36.03	33.56	31.64	29.97	28.21	26.19	0.9901	0.9821	0.9700	0.9535	0.9255	0.8728
Bridge	NSDD	28.93	27.22	25.78	24.26	22.94	21.38	0.9630	0.9384	0.9043	0.8505	0.7750	0.6716
	AOP	30.09	28.07	26.20	24.63	23.05	21.71	0.9781	0.9587	0.9254	0.8602	0.7848	0.6354
	LOTV	25.40	24.78	24.18	23.53	22.76	21.61	0.8950	0.8730	0.8444	0.8086	0.7589	0.6725
	ROR-NLM	28.91	26.91	25.48	24.25	23.56	22.57	0.9711	0.9480	0.9262	0.8938	0.8382	0.7870
	SAFE	26.65	26.40	25.75	25.04	23.66	22.50	0.9277	0.9260	0.9096	0.8867	0.8215	0.7593
	Algorithm 1	31.37	29.06	27.38	25.84	24.23	22.87	0.9823	0.9660	0.9456	0.9138	0.8633	0.7908

Table 2 PSNR and SSIM values of restoration results for images corrupted by random-valued noise (continued)

Image	Method	PSNR					SSIM						
		10%	20%	30%	40%	50%	60%	10%	20%	30%	40%	50%	60%
Mandrill	NSDD	25.30	24.03	22.92	21.71	21.04	20.22	0.9282	0.8917	0.8489	0.7756	0.6945	0.6064
	AOP	25.75	24.29	23.00	21.89	21.05	20.17	0.9454	0.9176	0.8727	0.7944	0.7172	0.6144
	LOTV	21.22	21.02	20.87	20.66	20.47	20.11	0.7536	0.7265	0.6999	0.6672	0.6289	0.5740
	ROR-NLM	25.23	23.74	22.51	21.54	20.73	20.26	0.9355	0.9036	0.8651	0.8153	0.7221	0.6607
	SAFE	24.55	24.25	22.41	21.48	20.88	20.03	0.9225	0.9160	0.8456	0.7840	0.7383	0.6692
	Algorithm 1	27.67	25.36	23.78	22.43	21.39	20.75	0.9606	0.9272	0.8863	0.8324	0.7728	0.6891
Couple	NSDD	30.20	28.47	27.25	26.27	24.79	23.26	0.9713	0.9434	0.9296	0.9013	0.8465	0.7691
	AOP	30.10	28.63	27.22	25.88	24.48	23.02	0.9879	0.9753	0.9555	0.9036	0.8564	0.7884
	LOTV	25.97	25.44	24.87	24.31	23.45	22.61	0.9599	0.9476	0.9316	0.9096	0.8781	0.8290
	ROR-NLM	28.44	26.91	25.93	25.39	24.55	23.71	0.9773	0.9565	0.9380	0.9261	0.9077	0.8659
	SAFE	29.38	28.04	27.70	26.98	25.53	24.20	0.9797	0.9698	0.9600	0.9473	0.9121	0.8587
	Algorithm 1	30.75	29.15	27.94	26.73	25.59	24.38	0.9882	0.9798	0.9694	0.9522	0.9281	0.8760
Plane	NSDD	32.92	30.93	29.26	27.57	25.75	23.67	0.9737	0.9580	0.9406	0.9127	0.8703	0.7476
	AOP	35.69	32.22	29.92	27.31	25.50	23.82	0.9952	0.9844	0.9636	0.9356	0.8929	0.8389
	LOTV	28.09	27.51	26.90	26.11	25.27	23.92	0.9768	0.9686	0.9581	0.9421	0.9188	0.8566
	ROR-NLM	30.91	29.91	29.04	27.79	26.89	25.35	0.9807	0.9738	0.9671	0.9568	0.9449	0.9178
	SAFE	28.81	28.60	27.83	26.55	26.28	25.24	0.9800	0.9686	0.9444	0.9006	0.9391	0.9048
	Algorithm 1	37.26	34.59	32.58	30.41	28.12	25.86	0.9948	0.9907	0.9849	0.9730	0.9548	0.9128

are set as suggested by the original authors. For NSDD, AOP, L0TV, and ROR-NLM, we assume that the original images are given. Then the parameter λ and iteration number in these methods are manually selected to achieve the highest PSNR values of the restored images.

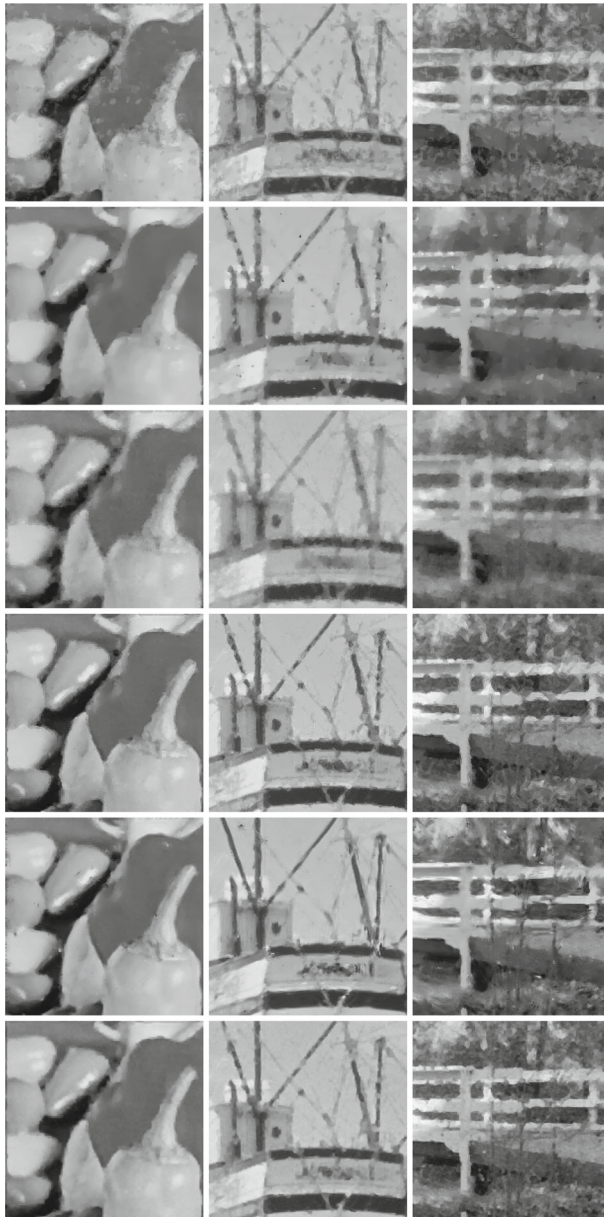


Fig. 5 Restoration results of different methods for test images Pepper, Boat and Bridge corrupted by 60% random-valued noise. From top to bottom: NSDD, AOP, L0TV, ROR-NLM, SAFE and Algorithm 1

3.1 Experimental setup for Algorithm 1

The proposed Algorithm 1 contains a few free parameters. Fortunately, these parameters are robust to test images and noise levels. We are able to use almost the same parameters for all experiments presented in this paper. In the following, we give some guidelines on choosing them.



Fig. 6 Restoration results of different methods for test images Mandrill, Couple and Plane corrupted by 60% random-valued noise. From top to bottom: NSDD, AOP, L0TV, ROR-NLM, SAFE and Algorithm 1

The stability of scheme (6) is favored with time step $0 < \tau \leq 0.25$. We let $\tau = 0.25$. The constant K needs to be small so that edges and small details are preserved in the restored images. We choose $K = 7$ for all experiments. The Perona–Malik type diffusivity involves the convolution operator. We use the MATLAB function “ $H = \text{fspecial}('gaussian', h, \sigma)$ ” to create the Gauss kernel and the MATLAB function “ $G = \text{imfilter}(IMG, H)$ ” to create the smooth version of image “ IMG ”. Two parameters h and σ are needed to be selected in the function “ fspecial ”. Numerical experiments show that the proposed filter is not sensitive to both parameters. We use $h = 3$ and $\sigma = 1.5$ for all experiments presented in this paper. It should be noticed that the denoising results can be improved by using $h = 5$ for extremely high level impulse noise. $\alpha = 2$ is selected based on empirical observation for better performance.

The MATLAB function “ medfilt2 ” is used for the median filter in step 5. The filter window ω of “ medfilt2 ” depends slightly on the noise level. We can simply choose $\omega = 3$ for noise level $s < 50\%$ and choose $\omega = 5$ for $s \geq 50\%$. The convolution operator in step 9 is set precisely the same as that of in the Perona–Malik type diffusivity. At last, we observe that the iteration number N increases with the increasing noise level s . We set $N = 20 \times s$.

3.2 Image denoising results

We now present the denoising results of all methods when test images are corrupted by 10% – 60% random-valued noise.

Table 2 lists the PSNR values and SSIM values of denoised images for all methods, where the highest values are shown in boldface. The PDE-based method NSDD performs not bad when the noise level is high. However, with the decrease of the noise level, the performance of NSDD drops rapidly. The variational method AOP has higher PSNR and SSIM values than another variational method LOTV for low noise level. This is because the noise candidate set \mathcal{D} is updated in AOP. While with the increase of the noise level, the advantage of the l_0 -norm in LOTV begins to emerge, which leads to higher PSNR and SSIM values than AOP. Nonlocal means filters SAFE and ROR-NLM both outperform variational methods for high noise level. And the results of SAFE are slightly better than the results of ROR-NLM. It can be observed that the proposed model has the highest PSNR and SSIM values in most cases.

The visual results of different methods for four test images corrupted by 60% random-valued noise is shown in Figs. 5 and 6. NSDD restores edges well. However, impulse noise is removed incompletely. Both AOP and LOTV use the TV regularization. Consequently, edges are well restored. They also cause the over smoothness of homogeneous regions. The

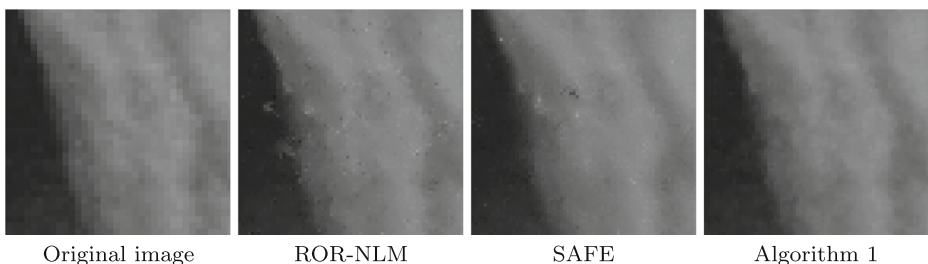


Fig. 7 Denoising results of ROR-NLM, SAFE and Algorithm 1 for restoring Boat image corrupted by 60% random-valued noise. The displayed region is (358 : 428, 183 : 253)

utilization of the nonlocal means filter leads to good visual equality, especially for Mandrill image that contains texture information. The proposed equation has the best compromise between noise suppression and dege/detail preserving.

The main advantage of the proposed equation is the ability to remove random-valued noise that is difficult to be detected. In Fig. 7, we observe that small impulse noise has remained in the result of the two-stage method ROR-NLM. SAFE, which uses the iterative structure-adaptive fuzzy estimation, can also not remove small impulse noise perfectly. No noise is observed in the result of the proposed equation.

4 Conclusion and discussion

A nonlinear diffusion equation with the regularized Perona–Malik diffusivity and a gray level based diffusivity has been proposed for the removal of random-valued impulse noise in images. The gray level based diffusivity has been constructed to estimate the amplitude of the noise, which is particularly suitable for removing random-valued noise. Numerical experiments showed that our equation removes random-valued noise that is difficult to be detected and outperforms recent PDE-based methods and nonlocal methods.

The proposed equation utilizes local information (i.e., four nearest pixels) for the restoration. It is not surprising that it has unsatisfied results compared to the nonlocal methods in particular cases. Nonlocal diffusion model that restores noisy images by the high degree of redundancy of natural images, is a straightforward generalization of the classical diffusion model. By replacing the classical diffusion operator in the proposed equation by the corresponding nonlocal diffusion operator, we expect to deduce a new model that inherits the advantage of nonlocal methods and has better denoising performance.

Acknowledgements The authors would like to thank Ming Yan for sharing his code of AOP with us and thank Yang Chen for sharing his code of SAFE with us. The author would also like to thank the referees for the valuable suggestions and comments. This work was supported by the National Natural Science Foundation of China (12001509) and the Natural Science Foundation of Zhejiang Province (LQ21A010010).

References

1. Adam T, Paramesran R, Mingming Y, Ratnavelu K (2021) Combined higher order non-convex total variation with overlapping group sparsity for impulse noise removal. *Multimed Tools Appl* 80(12):18503–18530
2. Andreadis I, Louverdis G (2004) Real-time adaptive image impulse noise suppression. *IEEE Trans Instrum Meas* 53(3):798–806
3. Arya K et al (2020) A new fuzzy rule based pixel organization scheme for optimal edge detection and impulse noise removal. *Multimed Tools Appl*:79
4. Aubert G, Kornprobst P (2006) *Mathematical problems in image processing: partial differential equations and the calculus of variations*, vol. 147 Springer Science & Business Media
5. Bresson X, Chan TF (2008) Fast dual minimization of the vectorial total variation norm and applications to color image processing. *Inverse Probl Imaging* 2(4):455–484
6. Buades A, Coll B, Morel JM (2005) A non-local algorithm for image denoising. In: *Computer vision and pattern recognition, 2005. CVPR 2005. IEEE computer society conference on*, vol. 2, pp. 60–65. IEEE
7. Catté F, Lions PL, Morel JM, Coll T (1992) Image selective smoothing and edge detection by nonlinear diffusion. *SIAM J Numer Anal* 29(1):182–193
8. Chan TF, Shen JJ (2005) *Image processing and analysis: variational, PDE, wavelet, and stochastic methods*, vol. 94. Siam

9. Chen HC, Wang WJ (2009) Efficient impulse noise reduction via local directional gradients and fuzzy logic. *Fuzzy Sets Syst* 160(13):1841–1857
10. Chen T, Wu HR (2001) Adaptive impulse detection using center-weighted median filters. *IEEE Signal Process Lett* 8(1):1–3
11. Chen J, Zhan Y, Cao H, Xiong G (2019) Iterative grouping median filter for removal of fixed value impulse noise. *IET Image Process* 13(6):946–953
12. Chen Y, Zhang Y, Shu H, Yang J, Luo L, Coatrieux JL, Feng Q (2018) Structure-adaptive fuzzy estimation for random-valued impulse noise suppression. *IEEE Trans Circuits Syst Video Technol* 28(2):414–427
13. Dong Y, Chan RH, Xu S (2007) A detection statistic for random-valued impulse noise. *IEEE Trans Image Process* 16(4):1112–1120
14. Goel N, Kaur H, Saxena J (2020) Modified decision based unsymmetric adaptive neighborhood trimmed mean filter for removal of very high density salt and pepper noise. *Multimed Tools Appl* 79(27):19739–19768
15. Gonzalez RC, Woods RE (2002) *Digital image processing second edition* Beijing: Publishing House of Electronics Industry, 455
16. Guo Z, Sun J, Zhang D, Wu B (2012) Adaptive Perona-Malik model based on the variable exponent for image denoising. *IEEE Trans Image Process* 21(3):958–967
17. Hosseini H, Hessar F, Marvasti F (2015) Real-time impulse noise suppression from images using an efficient weighted-average filtering. *IEEE Signal Process Lett* 22(8):1050–1054
18. Hosseini H, Marvasti F (2013) Fast restoration of natural images corrupted by high-density impulse noise. *EURASIP J Image Video Process* 2013(1):15
19. Hsieh MH, Cheng FC, Shie MC, Ruan SJ (2013) Fast and efficient median filter for removing 1–99% levels of salt-and-pepper noise in images. *Eng Appl Artif Intell* 26(4):1333–1338
20. Hwang H, Haddad RA (1995) Adaptive median filters: new algorithms and results. *IEEE Trans Image Process* 4(4):499–502
21. Ibrahim H, Kong NSP, Ng TF (2008) Simple adaptive median filter for the removal of impulse noise from highly corrupted images. *IEEE Trans Consum Electron* 54(4):1920–1927
22. Lee CS, Kuo YH, Yu PT (1997) Weighted fuzzy mean filters for image processing. *Fuzzy Sets Syst* 89(2):157–180
23. Liu L, Chen CP, Zhou Y, You X (2015) A new weighted mean filter with a two-phase detector for removing impulse noise. *Inf Sci* 315:1–16
24. Liu J, Ni A, Ni G (2020) A nonconvex $l_1(l_1 - l_2)$ model for image restoration with impulse noise. *J Comput Appl Math* 112934:378
25. Luo W (2005) A new efficient impulse detection algorithm for the removal of impulse noise. *IEICE Transactions on Fundamentals of Electronics. Commun Comput Inf Sci* 88(10):2579–2586
26. Luo W (2006) An efficient detail-preserving approach for removing impulse noise in images. *IEEE Signal Process Lett* 13(7):413–416
27. Meng X, Lu T, Min F, Lu T (2021) An effective weighted vector median filter for impulse noise reduction based on minimizing the degree of aggregation. *IET Image Process* 15(1):228–238
28. Nikolova M (2004) A variational approach to remove outliers and impulse noise. *J Math Imaging Vis* 20(1-2):99–120
29. Perona P, Malik J (1990) Scale-space and edge detection using anisotropic diffusion. *IEEE Trans Pattern Anal Mach Intell* 12(7):629–639
30. Roy A, Singha J, Manam L, Laskar RH (2017) Combination of adaptive vector median filter and weighted mean filter for removal of high-density impulse noise from colour images. *IET Image Process* 11(6):352–361
31. Rudin LI, Osher S, Fatemi E (1992) Nonlinear total variation based noise removal algorithms. *Phys D: Nonlinear Phenom* 60(1-4):259–268
32. Schulte S, Nachtgeal M, De Witte V, Van der Weken D, Kerre EE (2006) A fuzzy impulse noise detection and reduction method. *IEEE Trans Image Process* 15(5):1153–1162
33. Shen J, Chan TF (2002) Mathematical models for local nontexture inpaintings. *SIAM J Appl Math* 62(3):1019–1043
34. Shi K, Dong G, Guo Z (2020) Cauchy noise removal by nonlinear diffusion equations. *Comput Math with Appl* 80(9):2090–2103
35. Shi K, Guo Z, Dong G, Sun J, Zhang D, Wu B (2015) Salt-and-pepper noise removal via local hölder seminorm and nonlocal operator for natural and texture image. *J Math Imaging Vis* 51(3):400–412
36. Shi K, Zhang D, Guo Z, Sun J, Wu B (2016) A non-divergence diffusion equation for removing impulse noise and mixed gaussian impulse noise. *Neurocomputing* 173:659–670

37. Wang Z, Bovik AC, Sheikh HR, Simoncelli EP (2004) Image quality assessment: from error visibility to structural similarity. *IEEE Trans Image Process* 13(4):600–612
38. Wu J, Tang C (2011) PDE-Based random-valued impulse noise removal based on new class of controlling functions. *IEEE Trans Image Process* 20(9):2428–2438
39. Wu J, Tang C (2014) Random-valued impulse noise removal using fuzzy weighted non-local means. *SIViP* 8(2):349–355
40. Xiong B, Yin Z (2012) A universal denoising framework with a new impulse detector and nonlocal means. *IEEE Trans Image Process* 21(4):1663–1675
41. Yan M (2013) Restoration of images corrupted by impulse noise and mixed gaussian impulse noise using blind inpainting. *SIAM J Imaging Sci* 6(3):1227–1245
42. Yang J, Zhang Y, Yin W (2009) An efficient TVL1 algorithm for deblurring multichannel images corrupted by impulsive noise. *SIAM J Sci Comput* 31(4):2842–2865
43. Yuan G, Ghanem B (2017) l_0 TV: A sparse optimization method for impulse noise image restoration. *IEEE Trans Pattern Anal Mach Intell* 41(2):352–364
44. Zhang X, Bai M, Ng MK (2017) Nonconvex-TV based image restoration with impulse noise removal. *SIAM J Imaging Sci* 10(3):1627–1667
45. Zhang X, Xiong Y (2009) Impulse noise removal using directional difference based noise detector and adaptive weighted mean filter. *IEEE Signal Process Lett* 16(4):295–298
46. Zhang B, Zhu G, Zhu Z (2020) A TV-log nonconvex approach for image deblurring with impulsive noise. *Signal Process* 107631:174
47. Zhou Z (2012) Cognition and removal of impulse noise with uncertainty. *IEEE Trans Image Process* 21(7):3157–3167

Publisher's note Springer Nature remains neutral with regard to jurisdictional claims in published maps and institutional affiliations.